Hybrid particle-field molecular dynamics simulations for dense polymer systems

Giuseppe Milano[1,2,a)] and Toshihiro Kawakatsu[3]
[1]*Dipartimento di Chimica, Università di Salerno, via Ponte don Melillo Fisciano Salerno I-84084, Italy*
[2]*NANOMATES, Research Centre for NANOMAterials and nanoTEchnology at Salerno University, Italy*
[3]*Department of Physics, Tohoku University, Aoba, Aramaki, Aoba-ku, Sendai 980-8578, Japan*

(Received 25 March 2009; accepted 29 April 2009; published online 4 June 2009)

We propose a theoretical scheme for a hybrid simulation technique where self-consistent field theory and molecular dynamics simulation are combined (MD-SCF). We describe the detail of the main implementation issues on the evaluation of a smooth three-dimensional spatial density distribution and its special gradient based on the positions of particles. The treatments of our multiscale model system on an atomic scale or on a specific coarse-grained scale are carefully discussed. We perform a series of test simulations on this hybrid model system and compare the structural correlations on the atomic scale with those of classical MD simulations. The results are very encouraging and open a way to an efficient strategy that possess the main advantages common to the SCF and the atomistic approaches, while avoiding the disadvantages of each of the treatments. © *2009 American Institute of Physics*. [DOI: 10.1063/1.3142103]

I. INTRODUCTION

Atomistic simulations are powerful tools in the analysis and interpretation of the thermodynamics and microscopic structure of condensed matter and biological systems.[1] Actually, atomistic simulations based on semiempirical force fields adapted to every single substance on the basis of experimentally observed quantities are accurate and reliable.[2] This advantage of the atomistic simulations is accelerated by the fact that the computational power is increased by a factor of 10 at every 5 years. However, even with such rapidly increasing computational power, it is difficult to treat the huge number of degrees of freedom of the thermodynamic systems with the fully atomistic approaches when we investigate critically important phenomena on the mesoscopic scales such as self-assembly of biomolecules and relaxation of dense melts of high molecular weight polymer chains.

Coarse-grained generic models have been widely utilized in order to solve this problem.[3] The general strategy is to reduce the number of the degrees of freedom by coarse graining the models and keeping only those degrees of freedom that are relevant for a particular range of interest. In general, the price to pay for a coarse-grained model is the loss of microscopic chemical details.

Polymer dynamics is a very complex phenomenon with various dynamical modes and time scales involved and, in this respect, the coarse-graining techniques still are computationally demanding. Such a high demand on the computational power limits the time and length scales that can be addressed for relevant phenomena such as phase behavior of multicomponent systems. With this in mind, coarse-grained models can be considered as a basis for further approximations.

According to this spirit, Soga *et al.*[4] and Saphiannikova *et al.*[5] proposed self-consistent Brownian dynamics approaches to study coarse-grained models of polymer brushes. Later Ganesan and Pryamitsyn[6] proposed a further approach generalizing Doi's dynamical mean field theory of rodlike polymers by combining single chain Brownian dynamics algorithms with phenomenological prescriptions for the dynamics of coarse-grained field variables and they applied it to the study of the dynamical properties of polymer blend interfaces.[7] In these approaches, a substantial saving in computational time compared to previous coarse-grained techniques is achieved by adopting the self-consistent molecular field to calculate the interactions between the coarse-grained beads belonging to different polymer chains.

On the other hand, a particularly popular field-based approach is the self-consistent field (SCF) theory, where the mutual interactions between segments are decoupled and replaced by static external fields. In the SCF theories external fields, in turn, depend on the statistical average of the spatially inhomogeneous density distributions of particles created by the independent molecules interacting only with the external fields. Such external fields and the particle density distributions have to be determined self-consistently. Numerous applications to block copolymers,[8] proteins,[9] polymer composites,[10] and colloidal particles[11] have demonstrated that the SCF theory is a useful and powerful method.

Recently, Müller and Smith[12] extended the approach of Zuckermann, Pryamitsyn, and Ganesan in the framework of SCF theory by combining it with a Monte Carlo simulation of coarse-grained model of polymer chains to study phase separation in binary polymer mixtures. This approach has been widely and successfully applied by Müller and Daoulas to coarse-grained models of diblock copolymer thin films[13] and polymer nanocomposites.[14] Sides *et al.*[15] developed a similar hybrid particle-field method for coarse-grained mod-

a)Electronic mail: gmilano@unisa.it.

els of polymer nanocomposites based on the use of "cavity" functions to exclude the fluid components from the interior of solid particles.

With these precedents, the aim of the present paper is to develop a hybrid particle-field approach for molecular dynamics (MD-SCF) simulations and the relative implementation suitable for the treatment of atomistic force fields and/or specific coarse-grain models. The idea is to obtain a strategy, as far will be possible, having the main advantages and avoiding the main disadvantages of both SCF and atomistic approaches.

Molecular dynamics simulations are widely applied in the both fields of synthetic materials[16] and biomolecules.[17] Due to the possibility of straightforward chemically consistent models such as full atomistic or specific coarse-grained models these methods are very useful to characterize structural and dynamical properties of polymeric materials[18] and biomolecules.[19] The main disadvantage is the limitation to small length and time scales. Also in the best case of specific coarse-grain models the actual computer power limits the length scale to few tens of nanometers and few thousands of nanoseconds. In contrast, SCF approaches assure accessibility to definitely larger length and time scales but having models with very low chemical specificity.

This paper is organized as follows: In Sec. II, the basis of SCF theory useful to understand the present investigation and the derivation of a scheme suitable for hybrid particle-field molecular dynamics simulations are explained. In Sec. III, the implementation of the method, the scheme to obtain a smooth coarse-grained density functions and their special gradients from the particle positions are described. In Sec. IV, we show simulation results of two typical model systems.

II. FORMULATION OF THE SCF THEORY AND THE MOLECULAR DYNAMICS

In this section, a derivation of a theoretical scheme suitable for hybrid particle-field MD simulations is described. The section is also intended to quickly guide the reader to the basis of the SCF theory, which is useful in understanding the present investigation. For further details of the approaches on the mesoscopic scales, the readers should refer to Ref. 20.

The main issue, according to the spirit of SCF theory, will be to derive the partition function of a single molecule in an external potential $V(\mathbf{r})$ and to obtain a suitable expression of the $V(\mathbf{r})$ and its derivatives. In this formulation, the most computationally expensive part of the MD simulations, i.e., the evaluation of the nonbonded force and its potential between atoms of different molecules, can be replaced by evaluation for each atom of those with an external potential that depends on the local density at position $\boldsymbol{r}$.

In the framework of the SCF theory, a molecule is regarded to be interacting with the surrounding molecules not directly but through a mean field. According to this picture, we can split the Hamiltonian of a system of M molecules into two parts:

$$\hat{H}(\Gamma) = \hat{H}_0(\Gamma) + \hat{W}(\Gamma), \tag{1}$$

where Γ is used as shorthand for a set of positions of all atoms in the system, which specifies a point in the phase space. In Eq. (1) and also in the following, the symbol ˆ (hat) indicates that the associated physical quantity is a function of the microscopic states described by the phase space Γ. $\hat{H}_0(\Gamma)$ is the Hamiltonian of a reference ideal system composed of M noninteracting chains but with all the intramolecular interaction terms (bond, angle, nonbonded) that are usually considered in molecular simulations. On the other hand, the deviation from the reference system due to the intermolecular nonbonded interactions is accounted for by the term $\hat{W}(\Gamma)$ in Eq. (1).

Assuming the canonical (NVT) ensemble, the partition function of this system is given by

$$Z = \frac{1}{M!}\int d\Gamma \exp\{-\beta[\hat{H}_0(\Gamma) + \hat{W}(\Gamma)]\}. \tag{2}$$

The density distribution of atoms from microscopic point of view can be obtained considering that the microscopic density distribution can be defined as a sum of delta functions centered at the center of mass of each particle as

$$\hat{\phi}(\mathbf{r};\Gamma) = \sum_{p=0}^{M}\sum_{i=0}^{N_M} \delta(\mathbf{r} - r_i^{(p)}), \tag{3}$$

where M is the total number of molecules in the system and N_M is the number of particle contained in a molecule.

The deviation $\hat{W}(\Gamma)$ from the reference state $\hat{H}_0$ originates from the interactions between molecules. Here, we assume that $\hat{W}(\Gamma)$ depends on Γ only through the particle density $\hat{\phi}(\mathbf{r};\Gamma)$ as

$$\hat{W}(\Gamma) = \hat{W}(\hat{\phi}(\mathbf{r};\Gamma)). \tag{4}$$

Using the assumption Eq. (4) and the property of δ functional that obeys

$$\int D\{f(\mathbf{r})\}\delta[f(\mathbf{r}) - g(\mathbf{r})]F[g(\mathbf{r})] = F[f(\mathbf{r})], \tag{5}$$

we can rewrite the partition function in Eq. (2) as

$$Z = \frac{1}{M!}\int d\Gamma \int D\{\varphi(\mathbf{r})\}\delta[\varphi(\mathbf{r}) - \hat{\phi}(\mathbf{r};\Gamma)] \times \exp\{-\beta[\hat{H}_0(\Gamma) + W(\varphi(\mathbf{r}))]\}. \tag{6}$$

Using the Fourier representation of the delta functional, we obtain

$$\delta[\varphi(\mathbf{r}) - \hat{\phi}(\mathbf{r};\Gamma)] = \int D\{w(\mathbf{r})\} \times \exp\left[i\int w(\mathbf{r})(\varphi(\mathbf{r}) - \hat{\phi}(\mathbf{r};\Gamma))d\mathbf{r}\right]. \tag{7}$$

Inserting Eq. (7) into Eq. (6) leads to

$$Z = \frac{1}{M!}\int d\Gamma \int D\{\varphi(\mathbf{r})\} \int D\{w(\mathbf{r})\} \times \exp\left[i \int w(\mathbf{r})(\varphi(\mathbf{r}) - \hat{\phi}(\mathbf{r};\Gamma))d\mathbf{r} \right] \times \exp\{-\beta[\hat{H}_0(\Gamma) + W(\varphi(\mathbf{r}))]\}. \quad (8)$$

Now we define z as the partition function of a system made of a single molecule in an external potential $V(\mathbf{r}) \equiv i/\beta(w(\mathbf{r}))$ defined as

$$z[V(\mathbf{r})] = \int d\Gamma \exp\left\{ -\beta\left[\hat{H}_0(\Gamma) + \int \hat{\phi}(\mathbf{r};\Gamma) V(\mathbf{r}) d\mathbf{r} \right] \right\}. \quad (9)$$

Using this definition Eq. (9) and rearranging Eq. (8) we obtain

$$Z = \frac{1}{M!}\int d\Gamma \int D\{w(\mathbf{r})\} \exp\left\{ -\beta\left[-\frac{1}{\beta}\ln z + W(\varphi(\mathbf{r})) - \int V(\mathbf{r})\varphi(\mathbf{r}) d\mathbf{r} \right] \right\}. \quad (10)$$

In terms of this partition function, the mean field approximation is obtained by replacing the sum over the canonical ensemble in Eq. (10) with a Gaussian integral around the most probable state that minimizes the argument of the exponential function on the right side of Eq. (10).

The condition for the determination of the most probable state is given using functional derivatives:

$$\begin{cases} \dfrac{\delta}{\delta\phi(\mathbf{r})}\left\{ -\beta\left[-\dfrac{1}{\beta}\ln z + W(\varphi(\mathbf{r})) - \displaystyle\int V(\mathbf{r})(\varphi(\mathbf{r}))d\mathbf{r} \right] \right\} = 0 \\ \dfrac{\delta}{\delta V(\mathbf{r})}\left\{ -\beta\left[-\dfrac{1}{\beta}\ln z + W(\varphi(\mathbf{r})) - \displaystyle\int V(\mathbf{r})(\varphi(\mathbf{r}))d\mathbf{r} \right] \right\} = 0. \end{cases} \quad (11)$$

This leads to

$$\begin{cases} V(\mathbf{r}) = \dfrac{\delta W[\phi]}{\delta\phi(\mathbf{r})} \\ \varphi(\mathbf{r}) = -\dfrac{1}{\beta z}\dfrac{\delta z}{\delta V(\mathbf{r})} = \langle \hat{\phi}(\mathbf{r};\Gamma) \rangle = \phi(\mathbf{r}). \end{cases} \quad (12)$$

According to the derivation given above, now it is possible to obtain an expression for a density dependent external potential acting on each molecule.

If we assume that the interaction term W, where each component species is specified by an index K, the density dependent interaction potential takes the following form:

$$W[\{\phi_K(\mathbf{r})\}] = \int dr \left[\frac{k_B T}{2} \sum_{KK'} \chi_{KK'} \phi_K(\mathbf{r}) \phi_{K'}(\mathbf{r}) + \frac{1}{2\kappa}\left(\sum_K \phi_K(\mathbf{r}) - 1 \right)^2 \right], \quad (13)$$

where the second addend of the integrand of Eq. (13) is the relaxed incompressibility condition and κ is the compressibility that is assumed to be sufficiently small.

The corresponding mean field potential can be given by

$$V_K(\mathbf{r}) = \frac{\delta W[\{\phi_K(\mathbf{r})\}]}{\delta\phi_K(\mathbf{r})} = k_B T \sum_{K'} \chi_{KK'} \phi_{K'}(\mathbf{r}) + \frac{1}{\kappa}\left(\sum_K \phi_K(\mathbf{r}) - 1 \right). \quad (14)$$

In the case of a mixture of two components A and B, the mean field potential acting on a particle of type A at position $\boldsymbol{r}$ is given by

$$V_A(\mathbf{r}) = k_B T[\chi_{AA}\phi_A(\mathbf{r}) + \chi_{AB}\phi_B(\mathbf{r})] + \frac{1}{\kappa}(\phi_A(\mathbf{r}) + \phi_B(\mathbf{r}) - 1). \quad (15a)$$

Similarly, for a particle of type B is given by

$$V_B(\mathbf{r}) = k_B T[\chi_{BB}\phi_B(\mathbf{r}) + \chi_{AB}\phi_A(\mathbf{r})] + \frac{1}{\kappa}(\phi_A(\mathbf{r}) + \phi_B(\mathbf{r}) - 1). \quad (15b)$$

Then the force acting on the particle A at position $\mathbf{r}$ imposed by the interaction with the density field is

$$F_A(\mathbf{r}) = -\frac{\partial V_A(\mathbf{r})}{\partial \mathbf{r}} = -k_B T\left(\chi_{AA}\frac{\partial\phi_A(\mathbf{r})}{\partial\mathbf{r}} + \chi_{AB}\frac{\partial\phi_B(\mathbf{r})}{\partial\mathbf{r}} \right) - \frac{1}{\kappa}\left(\frac{\partial\phi_A(\mathbf{r})}{\partial\mathbf{r}} + \frac{\partial\phi_B(\mathbf{r})}{\partial\mathbf{r}} \right). \quad (16)$$

III. IMPLEMENTATION SCHEME

What is necessary in order to connect particle and field models is a scheme to obtain a smooth coarse-grained density function $\phi(\mathbf{r})$ directly from the particle positions Γ. Let us denote this procedure as

$$\bar{S}\{\hat{\phi}(\mathbf{r};\Gamma)\} = \phi(\mathbf{r}), \quad (17)$$

where $\bar{S}$ is a symbolic name of the mapping from the particle positions to the coarse-grained density. In this section, we will give an actual algorithm to perform this mapping.

The iteration scheme used in the proposed approach is outlined in Chart 1. The starting value of the density dependent mean field potential is obtained from the initial configuration of the system (at time t_0). The potential energy is the sum of the intramolecular interaction potentials (bond, angles, and intramolecular nonbonded) and the density dependent mean field potential. A new configuration is obtained by integrating the equation of motion of the particles from time t_0 to time $t_0+\Delta t$ [in our case we used the velocity Verlet algorithm as implemented in OCCAM (Ref. 21)]. At every prefixed density update time (Δt_{update}) the density is updated according to the updated positions of the particles in the simulation box. From the updated value of the density, a new value of the potential energy is calculated and then new forces are obtained. As outlined in Chart 1, the iteration scheme converges when the density and the potential become self-consistent.

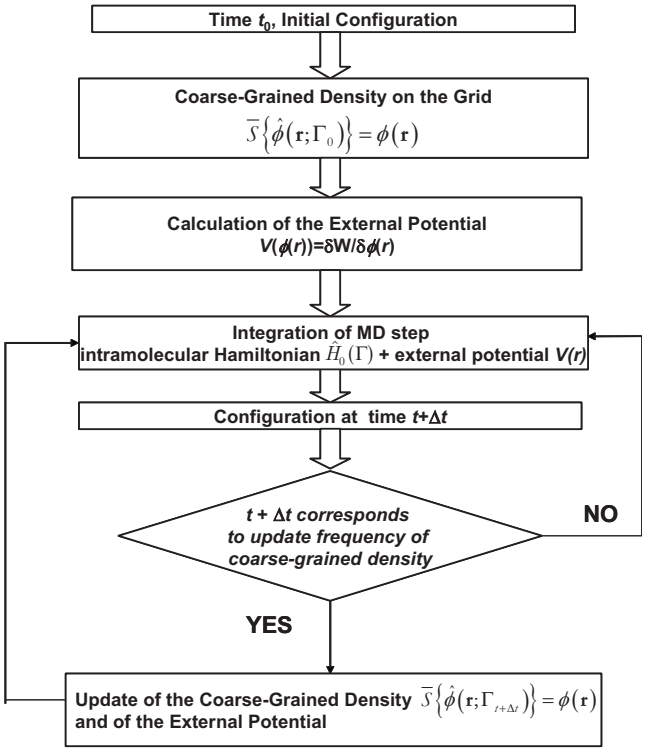

CHART 1. The iteration scheme proposed for hybrid MD-SCF simulations.

A. Coarse-grained density and density derivatives

In order to obtain a coarse-grained density, the simulation box is divided into $n\text{cell}=nx^*ny^*nz$ cells (where nx, ny, and nz are the number of cells in the x, y, and z directions). According to their positions in the simulation box, all the particles are distributed among these cells. In the implementation proposed here, the cell structure has been obtained using the method of "linked lists" that assures a rapid sorting of the particles.

The density and its derivatives used for the calculation of the forces and the potential energy due to particle-field interactions are both defined on three-dimensional lattice points obeying the periodic boundary conditions. The values of the density function at position $\boldsymbol{r}$ between lattice points are evaluated using linear interpolation of the values at neighbor latticed points.

Fractions of a particle are assigned to its neighbor mesh points according to the distances from the particle to the mesh points. There are several choices for this procedure. The lowest order choice is to assign each particle to its nearest neighbor mesh point. This procedure means that the system is divided into cubic cells whose centers locate at the lattice points and assign all the particles inside a cell to its center lattice point. A higher order alternative is to consider also the position of each particle inside the cell and to assign a fraction of this particle to each vertex of the cell.

To explain more easily the procedure, let us describe a two-dimensional case. An extension to three-dimensional mesh is straightforward. In Fig. 1, above-mentioned two strategies are compared. In the first case, according to the particle positions, value of the density in a cell is evaluated by counting the total number of particles in that cell. In the second case, according to the position of a given particle inside a cell, a fraction of it is assigned to the mesh points at the vertices of this cell. In this case the mesh points are not at the cell centers but at the vertices of the cell that are shared with the neighboring cells. As described in Fig. 2, the fraction of a particle assigned to a given vertex is proportional to the area of a rectangle whose diagonal is the line connecting the particle position and the mesh point on the opposite side of the cell. For instance a fraction $(l-x)^*(l-y)/l^2$ will be assigned to the mesh point 1 and a fraction of x^*y/l at mesh point 4 in Fig. 2. (l is the length of a side of the cell). In the present study, we choose the higher order scheme. The main reasons are following two: First, in the low order scheme, for a given number of particles in a cell, different configurations of particles inside the cell can give the same density. Thus the density field is rather insensitive to the local arrangement of the particles on the length scale of the mesh size l. Second, the use of the lower order scheme results in a stepwise

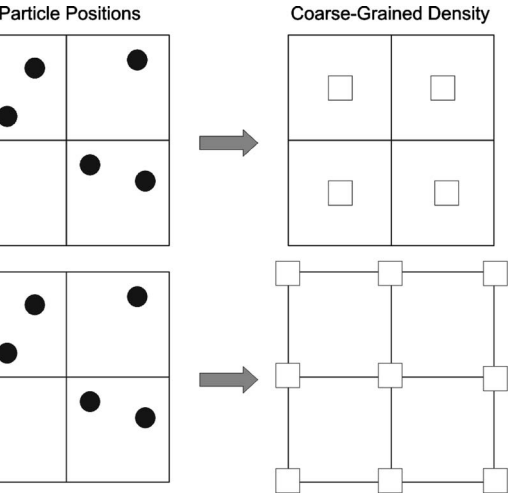

FIG. 1. Two strategies for the construction of a density grid are compared. In the first case, (top of the figure) according to the particle positions, value of the density in a cell is evaluated by counting the total number of particles in that cell. In the second case (higher order alternative) considering also the position of each particle inside the cell a fraction of this particle is assigned to each cell vertex.

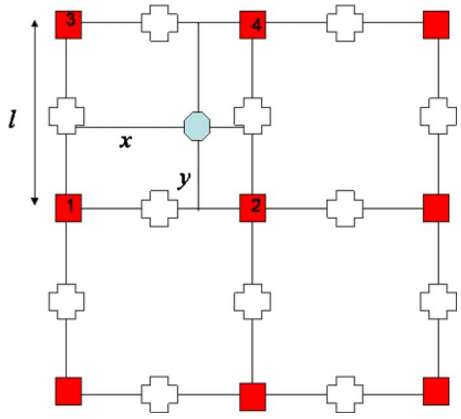

FIG. 2. (Color online) Geometry of particles fraction assignment in a two-dimensional case. The fraction assigned to a given vertex is proportional to the area of a rectangle whose diagonal is the line connecting the particle position and the mesh point on the opposite side of the cell.

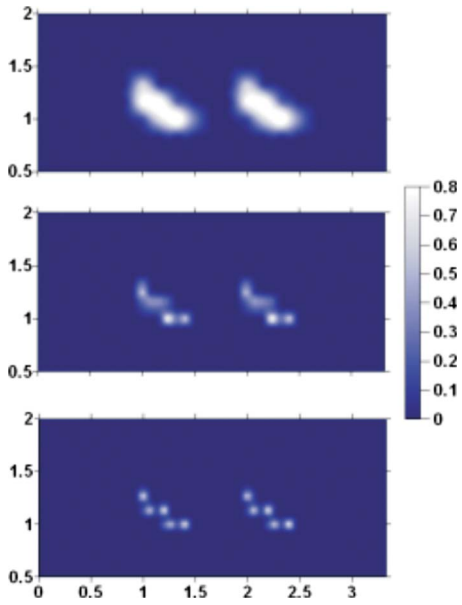

FIG. 3. (Color online) Two-dimensional density maps corresponding to a test configuration containing two *n*-pentane molecules in all *trans* conformation laying in the *xy* plane at different grid resolutions (starting from the top $l=1.66$, 0.83, and 0.66 Å).

variation of the density from one cell to its neighbor. On the contrary, it is smoother by distributing particle fractions over the vertices by using the higher order scheme.

In Fig. 3, we show three two-dimensional density maps corresponding to a test configuration containing two *n*-pentane molecules in all *trans* conformation lying in the *xy* plane at different grid resolutions (starting from the top $l=1.66$, 0.83, and 0.66 Å).

In Fig. 4, the geometry of assignment of the particle fraction is shown for the case of a three-dimensional lattice employed in this paper.

Spatial derivatives of the density distribution are defined on a staggered lattice (as indicated in Fig. 2 by cross symbols). As schematized in Figs. 4 and 5, the gray cubes indicate the lattice points where the density is defined. According to the choice of the definitions of the density at the center of each cell, the density gradients are defined on the center of each face (staggered lattice points) of the cube surrounding

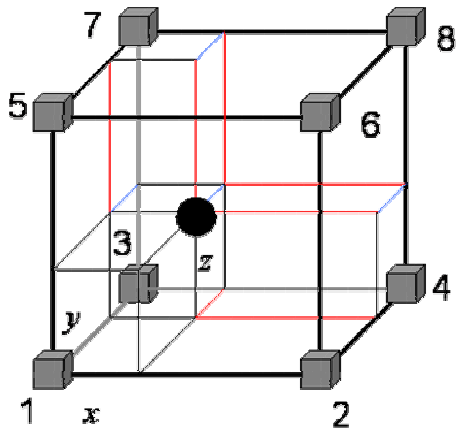

FIG. 4. (Color online) Schematized geometry of particle fraction assignment for the case of three-dimensional lattice employed in this paper.

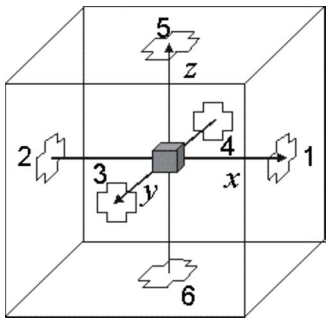

FIG. 5. Gradients defined on a staggered lattice, the density gradients are defined on the center of each face (staggered lattice points) of the cube surrounding a density lattice point (see Fig. 2, two-dimensional case, where crosses show the points on which the derivatives of the density are defined).

the density lattice point (see Fig. 5, where crosses show the six points on which the derivatives of the density are defined.).

Using the numbering of the staggered lattice points adopted in Fig. 5, the derivatives of the density in the x, y, and z directions can be interpolated in the following way:

$$\nabla_x\phi(x') = x'\nabla_x(1) + (1-x')\nabla_x(2),$$

$$\nabla_y\phi(y') = y'\nabla_y(3) + (1-y')\nabla_y(4), \tag{18}$$

$$\nabla_z\phi(z') = z'\nabla_z(5) + (1-z')\nabla_z(6).$$

In Eq. (18), the coordinate $\boldsymbol{r}' = (x', y', z')$ indicates the reference systems on the staggered lattice where the derivatives are defined. These lattice points are shifted from the density points according to the cell dimensions in the three directions of the space l_x, l_y, and l_z:

$$\nabla_x\phi(x) = \left(\left(x+\frac{l_x}{2}\right)/l_x\right)\nabla_x(1) + \left(\left(\frac{l_x}{2}-x\right)/l_x\right)\nabla_x(2),$$

$$\nabla_y\phi(y) = \left(\left(y+\frac{l_y}{2}\right)/l_y\right)\nabla_y(3) + \left(\left(\frac{l_y}{2}-y\right)/l_y\right)\nabla_y(4), \tag{19}$$

$$\nabla_z\phi(z) = \left(\left(z+\frac{l_z}{2}\right)/l_z\right)\nabla_z(5) + \left(\left(\frac{l_z}{2}-z\right)/l_z\right)\nabla_z(6).$$

IV. SIMULATIONS

In this section, the hybrid particle-field MD simulations are performed and their results are compared with those of the reference pure MD simulations. In the rest of this paper, we will refer these reference simulations as "particle-particle MD simulations."

A. Polymer model

As a first example, we consider a polymer melt. For the intramolecular interactions, we use a model in which the molecules are treated as a string of beads of mass m connected by harmonic springs and harmonic bending potentials.

$$\hat{V}_0(\Gamma) = \sum_{i=1}^{n\text{bonds}} \frac{k_{\text{bond}}}{2}(l-l_0)^2 + \sum_{i=1}^{n\text{angles}} \frac{k_\theta}{2}(\theta-\theta_0)^2 + \sum_{p=1}^{M} V_p^{\text{intramolecular nonbonded}}, \quad (20)$$

where k_{bond} is the bond force constant, and l and l_0 are the bond length and its equilibrium value, respectively. Similarly, k_θ is the angle force constant, and θ and θ_0 are the angle and its equilibrium value, respectively.

In each molecule, pair of atoms that are distant more than two bonds interact with a truncated and shifted Lennard-Jones excluded volume interaction denoted by $V_p^{\text{intramolecular nonbonded}}$. The superscript "intramolecular nonbonded" in Eq. (20) means that atom pairs included in the sum are chosen only inside the same molecule. The equilibrium value of the bond distance l_0 is chosen to be 0.40σ and the force constant $k_{\text{bond}}=300\,000\varepsilon$. For the bending potential, θ_0 is set to the tetrahedral value of 109.11° and the force constant $k_\theta=1500\varepsilon$. The simulations were performed with constant-*NVT* ensemble at density of $1.80\rho\ \sigma^3$ and at the reduced temperature $T^*=k_BT\varepsilon^{-1}=9.95$. These parameter values correspond to those of the united atom model of hydrocarbon chains with bond length 0.15 nm with the values of ε and σ comparable with OPLS force-field (Ref. 22) parameters ($\varepsilon=0.334$ kJ/mol, $\sigma=0.38$ nm) at density ~ 0.8 g cm^{-3} at $T=400$ K. We use a model of a polymer melt which contains 40 chains each of which is composed of 30 atoms. For a model of a block copolymer melt, we use a system composed of 320 chains each consisting of 30 atoms.

B. Simulation details

The MD program OCCAM (Ref. 21) was used to run the particle-particle simulations and a modified version of the same code was used for hybrid particle-field simulations. Both full particle-particle and particle-field hybrid MD simulations were run under constant-*NVT* conditions. The Berendsen thermostat with $\tau=0.02$ ps at a time step of 2 fs was used for full particle-particle MD simulations for the hybrid particle-field MD simulations (see the discussion below). The cutoff for nonbonded interactions is chosen to be $r_c=2.5\sigma$ with a Verlet neighbor list cutoff of 3.16σ. The same approach has been adopted for the intramolecular part of the interaction potential in the hybrid particle-field simulations. Both for the particle-particle and the particle-field simulations, production runs were performed up to 200 000 time steps.

C. Temperature control

In constant-*NVT* simulations, we implemented the temperature control according to the Berendsen thermostat.[23] This thermostat is one of the widely used techniques in atomistic molecular dynamics simulations.[24]

According to this thermostat, the velocities of the particles are scaled by a factor λ

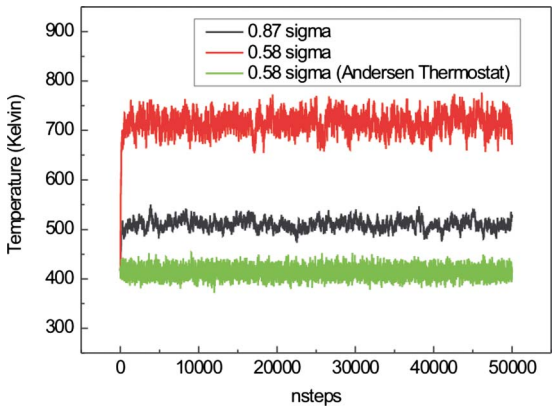

FIG. 6. (Color online) Temperature behavior in hybrid MD-SCF simulations at different density grid resolutions.

$$\lambda = \left[1 + \frac{\Delta t}{\tau}\left(\frac{T}{T_0} - 1\right)\right]^{1/2} \quad (21)$$

at every time step. Although this thermostat does not sample correctly the canonical ensemble, it is widely used because it is easy to implement and it assures temperature control in usual simulations. For recent discussions on thermostats in atomistic simulations, see Refs. 25 and 26.

The value of τ usually prescribed in order to give reliable temperature fluctuations is about ten times as the unit time step. In Fig. 6 the behavior of the temperature during constant-*NVT* simulations using τ with a value of ten times as the time step at different density resolutions is reported. From the figure it is clear that especially for simulations using higher resolution of the density, the temperature control is difficult. In particular, due to a more noisy density behavior, smaller cell sizes and stricter an incompressibility condition lead to more difficult temperature control.

This behavior can be ascribed to the choice of the Berendsen thermostat. Thermostats can be classified as either local or global. Local thermostats dissipate energy on a spatially localized scale. On the contrary, global thermostats dissipate energy uniformly in the system. In the present case we can consider the former as preferable because this is usually more realistic and (in principle) allows local temperature control. The simplest example of a local thermostat is the Andersen thermostat.[27] This thermostat assumes that the particles are undergoing collisions with "heat bath." Such a bath collision involves the assignment of a new velocity to the particle taken from the equilibrium Maxwellian distribution corresponding to the target temperature. In Andersen thermostat, particles have the probability $\Lambda\Delta t$ to have a collision with heat bath. This is described as

$$\mathbf{v}_i^*(t) = \begin{cases} \mathbf{v}_i(t), & \Lambda\Delta t < \zeta_1 \\ \eta, & \Lambda\Delta t \geq \zeta_1, \end{cases} \quad (22)$$

where η is a random vector

$$\eta = \sqrt{\frac{k_BT}{m_i}}[\zeta_2, \zeta_3, \zeta_4]. \quad (23)$$

In this scheme, ζ_1 is a uniform random number in $[0,1]$. The numbers $\zeta_2, \zeta_3, \zeta_4$ are independent random numbers taken

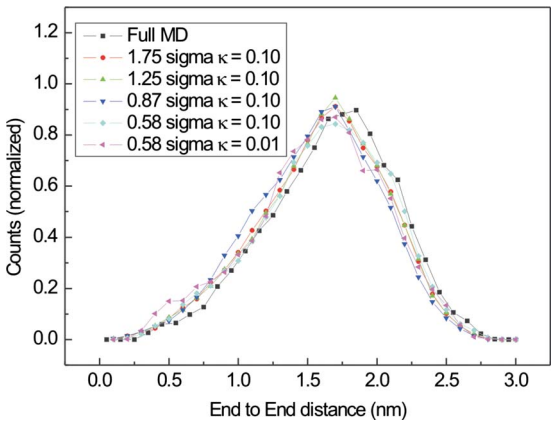

FIG. 7. (Color online) Probability distribution of end-to-end distances for different grid resolutions compared with the results of the particle-particle MD simulations.

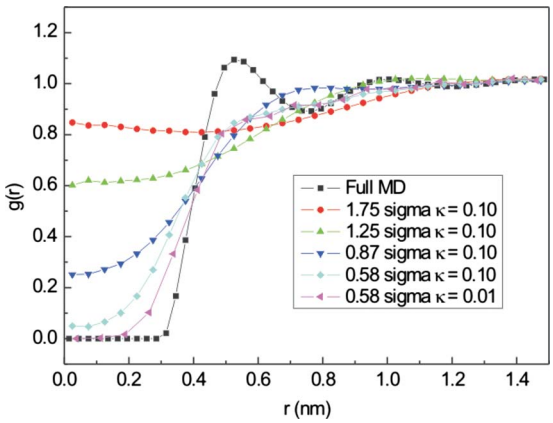

FIG. 8. (Color online) Atom-atom intermolecular radial distribution functions for different grid resolutions compared to the results of the particle-particle MD simulations.

from a Gaussian distribution of zero mean and unit variance.

In Fig. 6, we also report the behavior of the temperature in constant-*NVT* simulations using the Andersen thermostat with $\Lambda\Delta\tau=0.120$ (green curve), which corresponds to the most unfavorable case reported for the Berendsen thermostat (red curve). From the figure it is clear that the local thermostat works much better than the Berendsen one.

From these results it can be concluded that in the normal particle-particle simulations the use of the Berendsen thermostat does not show problems because part of its weakness is alleviated by collisions between particles approaching each other during the simulation. In the case of particle-field simulations, however, there are no collisions between particles, and therefore the weakness of the thermostat becomes critical. From this point of view, it is expected that the use of other global thermostats like the Berendsen thermostat, for example the Nosè–Hoover one,[28] would cause the same problems.

D. Homopolymer melt

The overall good reproduction of the structural properties of a single chain can be confirmed by comparing the probability distribution of end-to-end distance shown in Fig. 7 with the results of the particle-particle MD simulation.

In Fig. 8, the atom-atom intermolecular radial distribution functions are reported. In this figure, the radial distribution function of the particle-particle full MD simulations shows the typical behavior of a polymer melt, i.e., $g(r)$ has a correlation hole at short distances and a first peak followed by further oscillations at longer distance and finally reaches unity. The data shown in Fig. 8 indicate that the correlation between particles in the hybrid particle-field simulations is small if the lattice size is larger than about two times of σ. When the spatial resolution of the density filed becomes of the order as σ, the data in Fig. 8 show a deep correlation hole at short distances. The main differences in the behavior of the radial distribution functions between the particle-particle and hybrid particle-field simulations can be ascribed to the less stiff potential (for density resolutions larger than 0.6σ the $g(r)$ at $r=0$ starts from low but nonzero value and then grows less faster than that of the particle-particle one) and mean field approximation (reaches the value of 1 at large distances without the oscillations). Finally, in Fig. 8, we show the radial distribution function for a density resolution imposing a stiffer incompressibility condition ($\kappa=0.01$). Such a stiff incompressibility has an effect of avoiding superpositions between particles as can be observed in the $g(r)$ value between zero and 0.2 nm.

E. Block copolymer melt

As a further test of the proposed scheme, we simulate a melt of a block copolymer as an example of systems containing different species. In this case, our model for the intramolecular interactions is analogous to the one used by Murat *et al.*[29] The simulated system is a symmetric block copolymer melt composed of 320 chains each consisting of 30 atoms (15 of type *A* and 15 of type *B*). The simulations were performed with constant-*NVT* ensemble at density of $0.83\rho\sigma^3$ and at the reduced temperature $T^*=k_BT\varepsilon^{-1}=9.95$.

The mean field interaction parameters are chosen so that the system is in the strong segregation regime where a lamellar phase is stable as proved by theoretical considerations ($\chi_{AA}=\chi_{BB}=0$ and $\chi_{AB}=4.8$).[30] In Fig. 9, the time evolution of the self-consistent potential together with some configuration snapshots are shown. The starting configuration was obtained by simulating a completely homogeneous one-component system where the parameter χ_{AB} is set to zero. From Fig. 9, it is clear that during the simulation the self-consistent field potential monotonically decreases, which corresponds to a formation of domains of *A* or of *B* particles. After the first 50 000 time steps, the potential converges and beyond that time the self-consistent field shows fluctuations around its average value. From the snapshots, it is clear that the convergence of the potential corresponds to the formation of the lamellar phase.

V. CONCLUSIONS

A theoretical scheme for hybrid particle-SCF molecular dynamics simulations (MD-SCF) has been derived. The main implementation issues of such a hybrid particle-field method related to the building of a smooth three-dimensional spatial

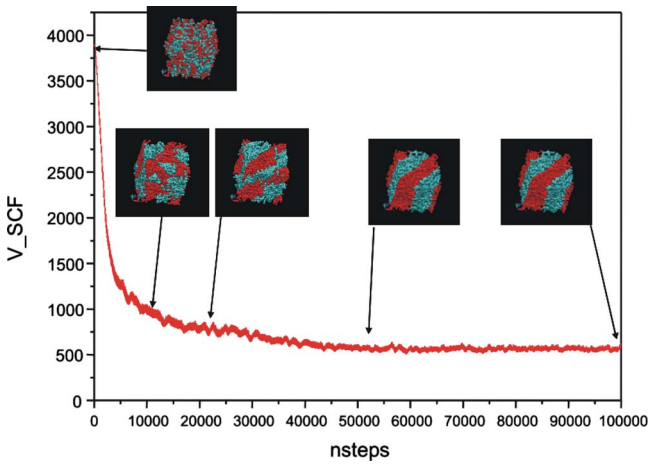

FIG. 9. (Color online) Symmetric block copolymer melt $A_{15}B_{15}$. Time evolution of the self-consistent potential together with some configuration snapshots are. The mean field interaction parameters ($\chi_{AA}=\chi_{BB}=0$ and $\chi_{AB}=4.8$) are chosen so that the system is in the strong segregation regime where a lamellar phase is stable.

function of density and its spatial derivatives from the particles positions and the iteration scheme have been described in a detailed way.

Aspects related to the treatment of systems on the atomic or specific coarse-grain models scale have been treated. With this respect, model systems have been tested by evaluating the structural correlations at atomic scale and have been compared with those of the standard particle-particle molecular dynamics simulations. The results are very encouraging and open the way to have an efficient strategy, as far will be possible, having the main advantages and avoiding the main disadvantages of both SCF and atomistic approaches.

From the point of view of the parametrization (in particular, in relating the parameters at particle level to the ones at field level; i.e., the χ parameters), one of the very promising methods is the systematic and quantitative treatment of this problem by associating a scalar Flory–Huggins χ parameter directly with the interaction potentials in a binary mixture of point particles recently proposed by Titievsky and Rutledge.[31]

ACKNOWLEDGMENTS

G.M. thanks the Japan Society for the Promotion of Science (JSPS) for an invitation fellowship, Regione Campania (Legge 5 2005), and INSTM (PRISMA2007) for financial support. T.K. thanks the Grant-in-Aid for Science from the Ministry of Education, Culture, Sports, Science and Technology, Japan on the Priority Area "Soft Matter Physics."

[1] W. F. van Gunsteren and H. J. C. Berendsen, Angew. Chem., Int. Ed. Engl. **29**, 992 (1990); H. Sun, J. Phys. Chem. B **102**, 7338 (1998).
[2] D. A. Mooney, F. Müller-Plathe, and K. Kremer, Chem. Phys. Lett. **294**, 135 (1998); N. A. McDonald and W. L. Jorgensen, J. Phys. Chem. B **102**, 8049 (1998); G. Milano and F. Muller-Plathe, *ibid.* **108**, 7415 (2004).
[3] P.-G. De Gennes, *Scaling Concepts in Polymer Physics* (Cornell University Press, Ithaca, New York, 1979); M. E. Doi and S. F. Edwards, *The Theory of Polymer Dynamics* (Oxford University Press, New York, 1986).
[4] K. G. Soga, M. J. Zuckermann, and H. Guo, Macromolecules **29**, 1998 (1996); L. Miao, H. Guo, and M. J. Zuckermann, *ibid.* **29**, 2289 (1996).
[5] M. G. Saphiannikova, V. A. Pryamitsyn, and T. Cosgrove, Macromolecules **31**, 6662 (1998).
[6] V. Ganesan and V. Pryamitsyn, J. Chem. Phys. **118**, 4345 (2003).
[7] B. Narayanan, V. A. Pryamitsyn, and V. Ganesan, Macromolecules **37**, 10180 (2004).
[8] M. W. Matsen and M. Schick, Phys. Rev. Lett. **72**, 2660 (1994); F. Drolet and G. H. Fredrickson, *ibid.* **83**, 4317 (1999); G. H. Fredrickson, V. Ganesan, and F. Drolet, Macromolecules **35**, 16 (2002); Y. Lauw, F. A. M. Leermakers, and M. A. C. Stuart, J. Phys. Chem. B **110**, 465 (2006); D. Q. Ly, T. Honda, T. Kawakatsu, and A. V. Zvelindovsky, Macromolecules **41**, 4501 (2008).
[9] E. Dickinson, V. J. Pinfield, D. S. Horne, and F. A. M. Leermakers, J. Chem. Soc., Faraday Trans. **93**, 1785 (1997).
[10] A. C. Balazs, C. Singh, and E. Zhulina, Macromolecules **31**, 8370 (1998).
[11] J. R. Roan and T. Kawakatsu, J. Chem. Phys. **116**, 7283 (2002); **116**, 7295 (2002).
[12] M. Muller and G. D. Smith, J. Polym. Sci. Part B: Polym. Phys. **43**, 934 (2005).
[13] M. P. Stoykovich, M. Müller, S. O. Kim, H. H. Solak, E. W. Edwards, J. J. de Pablo, and P. F. Nealey, Science **308**, 1442 (2005); K. C. Daoulas, M. Muller, M. P. Stoykovich, S. M. Park, Y. J. Papakonstantopoulos, J. J. de Pablo, P. F. Nealey, and H. H. Solak, Phys. Rev. Lett. **96**, (2006).
[14] F. A. Detcheverry, H. M. Kang, K. C. Daoulas, M. Muller, P. F. Nealey, and J. J. de Pablo, Macromolecules **41**, 4989 (2008); H. Kang, F. A. Detcheverry, A. N. Mangham, M. P. Stoykovich, K. C. Daoulas, R. J. Hamers, M. Muller, J. J. de Pablo, and P. F. Nealey, Phys. Rev. Lett. **100**, (2008).
[15] S. W. Sides, B. J. Kim, E. J. Kramer, and G. H. Fredrickson, Phys. Rev. Lett. **96**, (2006).
[16] F. Muller-Plathe, ChemPhysChem **3**, 754 (2002); M. Praprotnik, L. Delle Site, and K. Kremer, Annu. Rev. Phys. Chem. **59**, 545 (2008).
[17] M. Karplus and G. A. Petsko, Nature (London) **347**, 631 (1990); W. F. van Gunsteren, D. Bakowies, R. Baron, I. Chandrasekhar, M. Christen, X. Daura, P. Gee, D. P. Geerke, A. Glattli, P. H. Hünenberger, M. A. Kastenholz, C. Ostenbrink, M. Schenk, D. Trzesniak, N. F. A. van der Vegt, and H. B. Yu, Angew. Chem., Int. Ed. **45**, 4064 (2006); S. J. Marrink, A. H. de Vries, and D. P. Tieleman, Biochim. Biophys. Acta **1788**, 149 (2009).
[18] G. Milano and F. Müller-Plathe, J. Phys. Chem. B **109**, 18609 (2005); T. Spyriouni, C. Tzoumanekas, D. Theodorou, F. Muller-Plathe, and G. Milano, Macromolecules **40**, 3876 (2007); V. A. Harmandaris, N. P. Adhikari, N. F. A. van der Vegt, and K. Kremer, *ibid.* **39**, 6708 (2006).
[19] L. Monticelli, S. K. Kandasamy, X. Periole, R. G. Larson, D. P. Tieleman, and S. J. Marrink, J. Chem. Theory Comput. **4**, 819 (2008).
[20] T. Kawakatsu, *Statistical Physics of Polymers* (Springer, Berlin, 2004).
[21] G. Milano, OCCAM 3.0, University of Salerno, 2007.
[22] W. L. Jorgensen, D. S. Maxwell, and J. Tirado-Rives, J. Am. Chem. Soc. **118** (45), 11225 (1996).
[23] H. J. C. Berendsen, J. P. M. Postma, W. F. v. Gunsteren, A. DiNola, and J. R. Haak, J. Chem. Phys. **81**, 3684 (1984).
[24] F. Mullerplathe, Comput. Phys. Commun. **78**, 77 (1993); W. R. P. Scott, P. H. Hunenberger, I. G. Tironi, A. E. Mark, S. R. Billeter, J. Fennen, A. E. Torda, T. Huber, P. Kruger, and W. F. van Gunsteren, J. Phys. Chem. A **103**, 3596 (1999); D. Van der Spoel, E. Lindahl, B. Hess, G. Groenhof, A. E. Mark, and H. J. C. Berendsen, J. Comput. Chem. **26**, 1701 (2005).
[25] A. Mudi and C. Chakravarty, Mol. Phys. **102**, 681 (2004).
[26] G. Z. Y. L. Mor, J. Comput. Chem. **29**, 1992 (2008).
[27] H. C. Andersen, J. Chem. Phys. **72**, 2384 (1980).
[28] S. Nose, J. Chem. Phys. **81**, 511 (1984); W. G. Hoover, Phys. Rev. A **31**, 1695 (1985).
[29] M. Murat, G. S. Grest, and K. Kremer, Macromolecules **32**, 595 (1999).
[30] M. W. Matsen and F. S. Bates, Macromolecules **29**, 7641 (1996).
[31] K. Titievsky and G. C. Rutledge, J. Chem. Phys. **128**, 124902 (2008).